Research Paper

Mechanical properties of anodic titanium films containing ions of Ca and P submitted to heat and hydrothermal treatment

Gabriel G. de Lima[a], Gelson B. de Souza[b], Carlos M. Lepienski[c], Neide K. Kuromoto[c],*

[a]Materials Research Institute, Athlone Institute of Technology, Athlone, Ireland
[b]Department of Physics, Universidade Estadual de Ponta Grossa – UEPG, Ponta Grossa, PR, 84030-900 Brazil
[c]Department of Physics, Universidade Federal do Paraná – UFPR, CP 19044, PR, 81531-990 Brazil

ABSTRACT

Anodic oxidation is a technique widely used to improve the bioactivity of Ti surface. In this study, micro-arc oxidation (MAO) was used to obtain an anodic film incorporating Ca and P ions to evaluate the effect of heat and hydrothermal treatment on the mechanical and *in vitro* bioactivity properties of these new layers. The MAO process was carried out using $(CH_3COO)_2Ca \cdot H_2O$ and $NaH_2PO_4 \cdot 2H_2O$ electrolytes under galvanostatic mode (150 mA/cm^2). The thermal treatments were made at 400 °C and 600 °C in air atmosphere while hydrothermal treatment was made in an alkaline water solution at 130 °C. These surfaces presented desired mechanical properties for biomedical applications owing to the rutile and anatase phases in the anodic film that are more crystalline after thermal treatments; which provided an increase in hardness values and lower elastic modulus. The dry sliding wear resistance increased by performing thermal treatments on the surfaces with one condition still maintaining the film after the test. Bioactivity was investigated by immersion in simulated body fluid during 21 days and hydroxyapatite was formed on all samples. Finally, lower values of contact angle were obtained for heat treated samples.

1. Introduction

The aging of worldwide populations is expanding faster than the last decade (Flaherty et al., 2007; Jin et al., 2015; Peine et al., 2015) and are significantly related to the increasing numbers of osteoporosis incidents. Fragility fractures owing to osteoporosis are one of the causes of mortality that implies social and economic burdens (Cummings and Melton, 2002; Serrano and Blasco, 2007). For these reasons, the substitution and regeneration of bone tissue take up important place in tissue engineering field.

Titanium (Ti) and its alloys are widely used in implants for presenting good mechanical properties and excellent biocompatibility. The main factor of using titanium as a biomaterial

*Corresponding author.
E-mail address: kuromoto@fisica.ufpr.br (N.K. Kuromoto).

from biocompatible metals is its low elastic modulus ($\sim$ 100 GPa) and, therefore, closer to the bone (10–40 GPa) (Niinomi, 2008). In addition, titanium has a layer of native oxide film which grows spontaneously on the surface on exposure to air (Kasemo, 1983) and determines the surface properties of a titanium implant. However, the concentration of hydroxyl groups in the oxide on the pure metal is very low. Thus, titanium surface modifications are necessary to make it bioactive. Surface modification can have different morphologies and varied properties of the substrate targeting specific applications (Liu et al., 2004; D. Wei et al., 2007).

Anodic oxidation, as surface modification for titanium oxide, has the advantage to produce an oxide layer with tailored properties, such as chemical and mechanical properties (Li et al., 2008). However, the oxide layer formed by the anodic oxidation presents bioactivity only if it is formed under dielectric breakdown (Yang et al., 2004). At voltages above the dielectric breakdown threshold, sparks occurs and the formed layer is more porous and less uniform. This process is known as micro-arc oxidation (MAO) or Plasma electrolytic oxidation (PEO). Using this technique, the best qualities of coatings can be synthesized with high hardness, adhesion strength and wear resistance than those obtained by the standard procedure (Yang et al., 2004). The coatings features can be controlled by adjusting the electrolyte parameters, such as temperature, composition, voltage, current, and time (Liu et al., 2004).

The literature has shown that the incorporation of ions in the oxide layer is beneficial for the nucleation kinetics of the hydroxyapatite (HA). Anodic films containing Ca and/or P ions induce new bone tissue and become bioactive (Laurindo et al., 2014; Liu et al., 2011; J. Wei et al., 2007). The bioactivity of oxide layers containing Ca and P depends on the existence of hydroxyl radicals and the release of Ca ions in the body fluid, raising the pH and the ionic activity factor. These features together favor the nucleation of hydroxyapatite (Chen et al., 2006). Anodic layers rich in Ca and P produced on Ti by MAO process also presents a significant improvement on corrosion resistance (Park et al., 2007).

de Souza et al. (2011) showed that anodic layers grown on titanium using electrolyte containing Ca–P present soft Ca–P rich areas, whereas the oxide layer itself had an elastic modulus close to the bone ($\sim$70 GPa). However, such Ca–P containing layer presented brittleness in scratch tests, which is removed under lower charge forces. The instability of the coating affects the stability of the prosthesis, since the generated particles cause inflammation at the implant site (Korkusuz and Korkusuz, 2004). In addition, recent studies show that due to heat or hydrothermal treatments on MAO films there is an improvement of the bioactivity of the films since the Ca ions incorporated in the oxidation process greatly affect the cellular response (Ryu et al., 2008; Yang et al., 2014). However, these studies with respect to anodic film obtained by MAO technique and subsequent thermal or hydrothermal treatment on surfaces containing Ca and P ions do not address important characteristics such as mechanical properties and corrosion resistance. These questions are relevant when the layers demand that is both bioactive and with needs to have good mechanical properties. Therefore, in the current study TiO_2 films were produced by anodic oxidation using Ca- and P-electrolytes based on the work carried out by de Souza et al. (2011) with posterior thermal and hydrothermal treatments to induce an improvement in the mechanical properties and bioactivity of these films.

2. Experimental

2.1. Sample preparation

Commercially pure titanium (grade 2, supplied by Ti Brazil – ASTM F67) samples were grounded using 400 and 600 SiC papers, followed by polishing with 6 µm diamond paste and colloidal silica suspension. The samples were successively washed with acetone, isopropyl alcohol, and distilled water in an ultrasonic cleaner for 30 min each step. The final dimension of the substrate was 10 mm × 10 mm × 1.0 mm.

The MAO process was made galvanostatically at room temperature in an electrolyte solution containing 0.14 mol/l calcium acetate monohydrate ((CH_3COO)$_2$Ca$\cdot$H$_2$O) and 0.06 mol/l sodium biphosphate dihydrate ($NaH_2PO_4 \cdot 2H_2O$) in deionized water. The current density was 150 mA/cm^2 for 100 s. The voltage was recorded during the test and it increases from zero to about 400 V. Micro arcs were observed during anodization process when voltage increases to higher values.

2.2. Heat treatment and hydrothermal treatment

The thermal and hydrothermal treatments were used in order to induce structural changes in the anodic layers and evaluate the effects of heating on the mechanical properties of Ti anodic film. The thermal treatment was done using a muffle furnace. Samples were divided into two groups and labeled appropriately:

Sample were heated at 5 °C/min up to 400° and 600 °C staying at these temperatures for 1 h and allowed to cool in the oven. Such temperatures were chosen for presenting the best results in accordance with the literature in terms of bioactivity (Tao et al., 2009; D. Wei et al., 2007). Hydrothermal treatment was performed in a conventional autoclave at 130 °C and P_{MAX} of 80 kPa. The samples were immersed in 50 ml falcon tubes with deionized water and addition of NaOH addition to adjust the pH value between 10–11, then the tubes were immersed in deionized water contained in an autoclave for 5 h (Alsaran et al., 2011; Vangolu et al., 2011).

Samples codes in this research paper are defined as AO – Anodic oxidation; AO+HT – Anodic oxidation with hydrothermal treatment; AO+TT400 °C – Anodic oxidation with thermal treatment at 400 °C; AO+TT600 °C – Anodic oxidation with thermal treatment at 600 °C.

2.3. Microstructure and morphology

The morphology of the investigated layers was analyzed using scanning electron microscopy (SEM) and the chemical composition using electron dispersive X-ray spectroscopy (EDS). The samples were previously sputtered with gold for 110 s at 0.1 mBar vacuum. Structural changes were characterized by X-ray diffraction (XRD) in θ–2θ geometry, using Cu K$_\alpha$

radiation and scan velocity 0.24 °/min. Also, grazing incidence x-ray diffraction (GIXRD) was used. The phase content (%) of the sample was calculated from the resulting diffractograms using the Spurr equation (Spurr and Myers, 1957):

$$W_R = \frac{I_R(1\ 1\ 0)}{0.8 I_A(1\ 0\ 1) + I_R(1\ 1\ 0)}$$

where I_A (101) and I_R (110) are the stronger peak intensities of anatase and rutile respectively, and W_R is the rutile mass fraction.

The average roughness (Ra) and layer thickness were determined using a stylus profilometer. The surface profile was integrated by the ensemble of 2000 data points assembled across the scan length of 1000 μm, in ten different surface sites.

2.4. Mechanical properties, scratch tests and tribology

Hardness and elastic modulus of surfaces were obtained by instrumented indentation, following the Oliver and Pharr method (Oliver and Pharr, 2004). The applied loads ranged between 0.14 mN and 400 mN in ten loading-unloading cycles, using a Berkovich type diamond indenter. At each sample, a matrix with 20 indentation sites separated by 100 μm was executed. Scratch tests were performed with the same indentation facility. The lateral displacement of the indenter was made in the direction of one of their edges. The scratches were made with a linear loading ramp 0–400 mN, at constant load rate. The scratch length was 600 μm and scratch speed was 10 μm/s. Five scratches per sample were made. Measurement of mechanical strength of the surface was performed by analysing the profiles scratching with SEM images.

Coefficient of friction and wear values were conducted with a linear reciprocating tribometer. Tests were performed at room temperature under unlubricated condition. Tungsten carbide ball WC (Co) with a diameter of 6 mm under load of 3 N was used at a sliding speed of 1 cm/s, half-amplitude of 1 mm and a sliding distance of 9 m. The load of 3 N was chosen since previous work in these type of films gives a reproducible result for friction coefficient and wear rate and can differentiate the samples in this work. Width and depth of the wear tracks were measured by a surface profilometer to calculate the worn volume of the samples. Wear rate of the samples was calculated in terms of $mm^3\,N^{-1}\,m^{-1}$ by dividing the worn volume by the normal load and the total sliding distance $K = V/(w \cdot s)$, where K is the value of the wear rate, V is the worn volume, w is the normal load, and s is the distance moved (Arslan et al., 2013).

2.5. Bioactivity

In vitro bioactivity tests were carried out by soaking the samples in a simulated body fluid solution (SBF) according to the preparation protocol and methodology applied in Kokubo and Takadama (2006). Each sample was placed in a falcon tube containing 50 ml of SBF solution, followed by bath incubation at 37 °C for a period of 21 days. After the set period of immersion, the samples were washed in distilled water and oven dried at 40 °C for 24 h. The degree of bioactivity was qualitatively estimated observing the sample surface. The bioactivity response is observed by the presence of hydroxyapatite on the samples, which can be detected by SEM/EDS analysis.

2.6. Wettability

In the present study the wettability was analyzed by measuring the contact angle using a goniometer, by the sessile drop method with SBF solution. The angle of the drop was measured at 15 s interval, over the integrated time of 400 s.

3. Results and discussion

3.1. Morphology

The SEM images of the Ti surfaces anodically oxidized and anodically oxidized with subsequent hydrothermal and heat treatments are shown in Fig. 1. The morphology of oxidized surface presents the well-known porous distribution and high roughness (Yang et al., 2004).

Pores with different sizes were observed in the same sample surface. These size of the pores are dependent on the growth rate of the anodic layer and the amount of sparks, resulting in larger pores for high arcing as compared to regions with little arcing (Yang et al., 2004). Dark and clear zones observed in the AO sample, as shown in Fig. 1a, are related to Ca and P distribution. According to de Souza et al. (2011) the dark regions are richer in Ca and P. Some surface cracks are also observed.

The elements in the anodic layers were identified by EDS analysis (Fig. 1e). The AO samples present Ca, P, Ti and O. The Ca and P were incorporated during the MAO process. The Ca and P content in AO+HT samples increased with Ca prevailing over P with a Ca/P relation of 1.6 that is typical for hydroxyapatite (HAp). In the literature it is reported that during hydrothermal treatment the phosphate ions binds to hydroxyl groups through hydrogen bond attracting Ca_2^+ ions forming hydroxyapatite (Alsaran et al., 2011). However, in this work HAp crystals were not observed by images or by X-Ray analysis. According to Vangolu et al., visible HAp crystals are shown for hydrothermal treatment in temperatures higher than 190 °C (Vangolu et al., 2011). In thermal treated samples, the EDS spectrum did not change compared to AO sample.

The average roughness and thickness of anodic layers (Table 1) shows that heat treatment slightly alters the surface roughness, showing no variations in layer thickness.

The cross-sectional views of the standard sample AO and AO+TT600 °C (Fig. 2) shows different morphologies. The standard anodic layers (Fig. 2a) exhibit a porous morphology of the TiO_2 and a Ca–P layer at the surface, similar morphologies have been reported (Li et al., 2005). The heat treated samples on the other hand (Fig. 2b), shows a reduced porous morphology, as compared to the surface.

3.2. XRD

XRD patterns to samples anodically oxidized with thermal and hydrothermal treatments (Fig. 3) indicate that heat
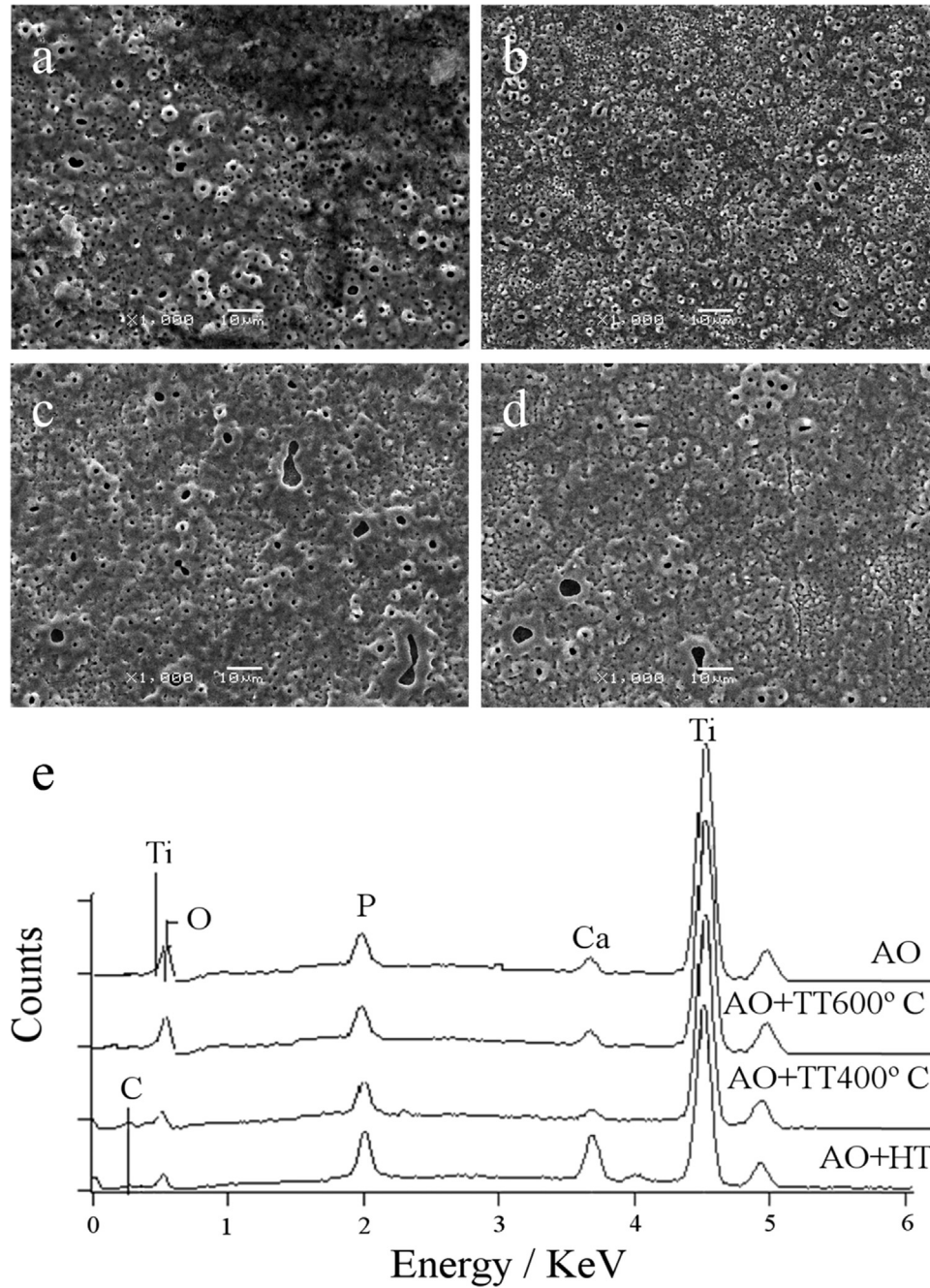
Fig. 1 – SEM images of the samples AO (a), AO+HT (b), AO+TT400 °C (c), AO+TT600 °C (d) and (e) EDS spectrum.

treatment increased the amount of anatase (JCPDS # 21-1272) and rutile (JCPDS # 21-1276) phases. Peaks corresponding to planes (101) ($\sim 25°$), (004) ($\sim 37°$), (200) ($\sim 47°$), (211) ($\sim 55°$) and, (204) ($\sim 58°$) were assigned to anatase while diffraction peaks were assigned to rutile for planes (110) ($\sim 27°$), (101) ($\sim 37°$), (111) ($\sim 41°$) and (211) ($\sim 54°$).

Samples submitted to hydrothermal treatment presented rutile phase in small quantity exhibiting 90% anatase and

Table 1 – Mechanical and tribological parameters of the studied samples.

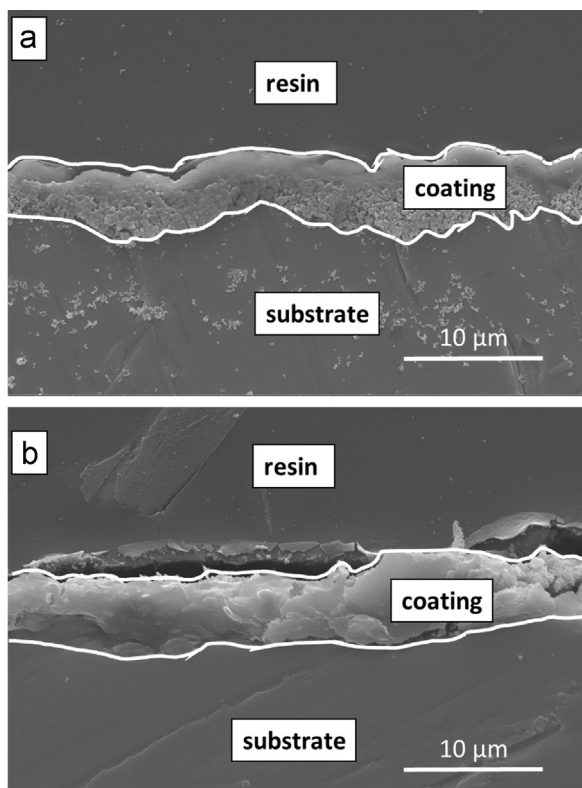| Sample code	Roughness (μm)	Layer thickness (μm)	Elastic modulus (GPa)	H/E	Wear rate (mm³/N/m)
AO	0.37 ± 0.05	3.6 ± 0.3	40 ± 5	0.10 ± 0.06	$1.1E^{-4} \pm 8E^{-5}$
AO+HT	0.41 ± 0.04	3.5 ± 0.5	158 ± 40	0.04 ± 0.01	$2.2E^{-4} \pm 8E^{-5}$
AO+TT400 °C	0.45 ± 0.05	3.7 ± 0.3	156 ± 18	0.05 ± 0.02	$3.5E^{-5} \pm 1E^{-5}$
AO+TT600 °C	0.47 ± 0.07	3.5 ± 0.4	147 ± 45	0.06 ± 0.02	$3.3E^{-6} \pm 1E^{-7}$

Fig. 2 – SEM cross-sectional views of (a) AO and
(b) AO+TT600 °C.

10% rutile in its structure. In addition, any trace of calcium phosphate peaks was identified in the AO+HT sample. The treatment time and temperature were lower than that used by other researchers who observed hydroxyapatite after hydrothermal treatment (Ryu et al., 2008).

Rutile and anatase phases appear in the anodic layer after heat treatments, 400 °C and 600 °C Fig. 3(b and c). Rutile ratio to anatase slightly increases with temperature, varying from 17% rutile and 80% anatase for 400 °C to 23% rutile and 77% anatase for 600 °C. Anatase-to-rutile transformation in titania

system is a metastable-to-stable irreversible transformation and has been described by the nuclear-size model effect (Kumar, 1995). During the heat treatment anatase crystals coarsen and when their size reaches a critical value they transform to stable rutile phase. Some authors (Chen et al., 2006; Montazeri et al., 2011; Zhou et al., 2014) have reported the presence of calcium phosphate crystals on thermal treated AO samples. However the X-ray diffraction did not show calcium phosphate phases or other containing Ca or P despite the existence of Ca and P in the anodized surfaces as detected by EDS similar to results reported by Ishizawa and Ogino (1995) and Ma et al. (2012). The results indicate that the heat treatment increased the crystallinity of the titanium oxide which is in agreement with literature (Jin et al., 2008; Tao et al., 2009).

3.3.   Mechanical properties

3.3.1.   Nanoindentation tests analysis
The results of hardness and elastic modulus measured on the studied surfaces are shown in Fig. 4. The results are influenced by substrate effect (Saha and Nix, 2002). Elastic and plastic deformation field can exceed the layer thickness after a certain amount of penetration depth, then the calculated hardness and elastic modulus correspond to the combination response of the film layer and the substrate (Saha and Nix, 2002). According to literature the most acceptable value for film hardness is obtained if the penetration depth is up one tenth of the film thickness (Fischer-Cripps, 2011). On the other hand, elastic modulus is affected by the substrate beneath even at very shallow depths. However, at the present case the evolution of hardness and elastic modulus through all the layer thickness were analyzed. It is observed that all hardness profiles decreased with increasing contact depth for low indenter penetrations.

The hardness values for the samples with heat treatment of 600 °C ($\sim$250 nm) was (6.2±1.5) GPa, whereas the reference sample (AO) values were (4.2±1.4). This trend was observed through all the analyzed profile up to $\sim$2700 nm, that is, the
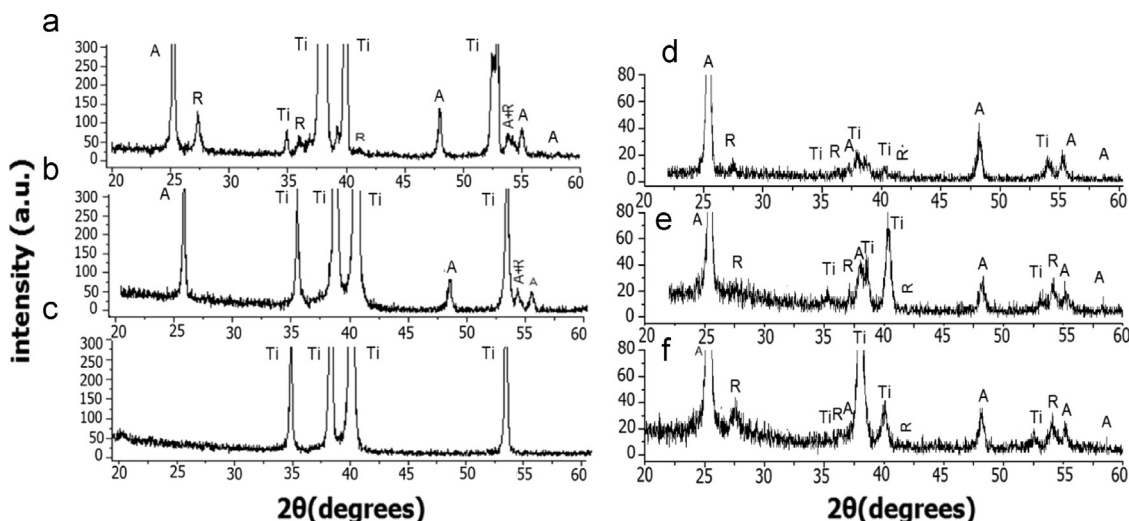

Fig. 3 – (Left) XRD diffractogram of (a) AO+TT600 °C, (b) AO, (c) Polished titanium. (Right) GIXRD patterns (grazing angle of 1.5°) for (d) AO+HT, (e) AO+TT400 °C (f) AO+TT600 °C. Ti=titanium; R=rutile; A=anatase.].
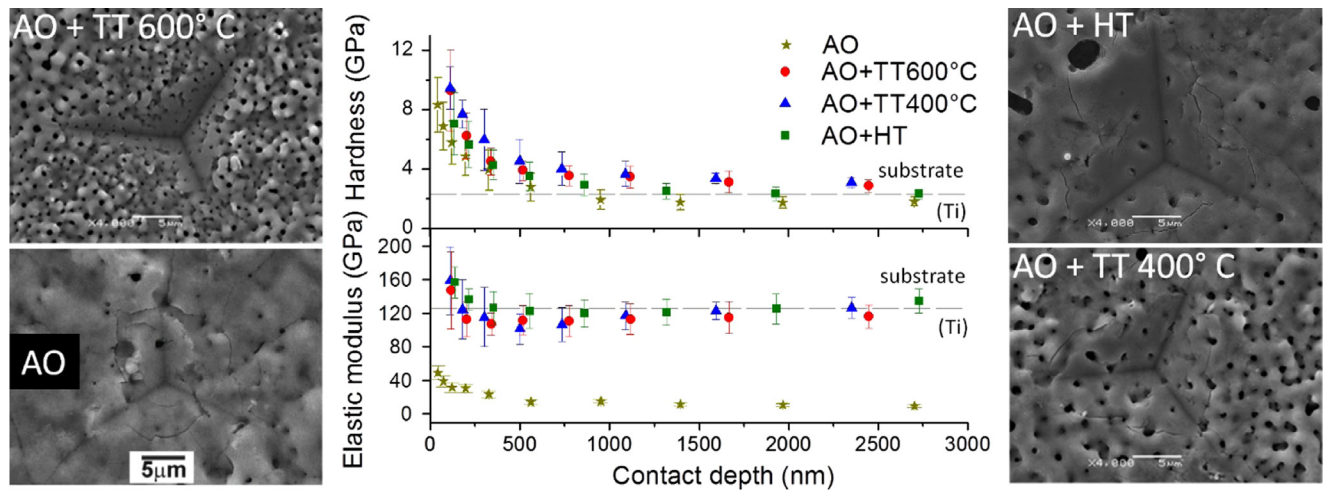
Fig. 4 – Elastic modulus and hardness profiles of anodically oxidized (AO), anodically oxidized+heat treatment 400 °C (AO+TT400 °C), anodically oxidized+heat treatment 600 °C (AO+TT600 °C), anodically oxidized+hydrothermal treatment (AO+HT). The dashed lines indicate the Ti bulk values. The SEM micrographs of indentation imprints produced with 400 mN applied load are also indicated on the figure.

sample AO+TT600 °C presented slightly higher hardness values. The same was valid for the AO+TT400 °C sample. The raise in hardness could be attributed by the effect of the heat treatment acting over the entire anodized layer, instead of the thin near surface region.

After heat treatments in 400 °C or 600 °C (at ~250 nm), hardness profiles were slightly higher than for the AO samples, although all of them presented large dispersion (large error bars) and were statistically similar. The dispersion could be explained mostly due to surface roughness. Another possible effect can be due to the crystallization of the components presented in the layers after heat treatment. The surface morphology affects the instrumented indentation results through errors caused in the determination of the contact depth during the tip and asperities interaction, notably under low loads and small penetration depths, as discussed elsewhere (de Souza et al., 2010). Likewise, the presence of pores in the perimeter of contact affects the plastic deformation field imposed by the incoming indenter. The observed dispersion in the hardness profiles can also be attributed to the structural conditions found in MAO layers.

The anatase to rutile transformation is a nucleation and growth process, which is time and temperature dependent (Hanaor and Sorrell, 2011; D. Wei et al., 2007). Thus, inner regions become inhomogeneous after heat treatment, leading to a rutile precipitation causing a hardening effect. Thus, different indentation sites may reach different precipitate concentrations. Such precipitates are harder than the anatase matrix (Hanaor and Sorrell, 2011), affecting the dislocations movement and the propagation of cracks (Meyers and Chawla, 1999), raising the overall layer hardness. After hydrothermal treatment, changes in the rutile to anatase ratio were not expected, since the HT temperature (130 °C) is much lower than the rate for the rutile precipitation and growth. However, the AO+HT hardness profile in Fig. 4 is similar to those samples submitted to the thermal treatment.

Fig. 4 also shows images of imprints left by the Berkovich indenter during the tests. The SEM images show lateral

cracks in AO sample resulting from the normal loading. It is conspicuous that TT layers present an increase in fracture toughness related to AO samples, since they present fewer cracks, and the layers integrity were preserved. Moreover, AO+HT samples had fewer cracks as compared to AO samples which could be possible due to an increase of crystalline phases described in XRD. Furthermore, the AO+TT600 °C sample has fewer or none cracks and a lower brittleness due to their increased crystallinity identified by XRD as compared with the AO+TT400 °C and AO+HT. Among the thermal treatments, the hydrothermal treatment showed that higher cracks are more brittle.

The heat treatment on the anodic layers that led to an increase on rutile, could also increase the residual stress, since rutile have more coefficient of expansion and density than anatase. However, the heat treatment can also reduce greatly the amount of residual stress on the standard anodic layer (Shen et al., 2013), the balance of these forces had an overall decrease of residual stress, resulting in less cracking anodic layer and increased values of hardness leading to an overall improved adhesive coating.

Elastic modulus of the AO layer was lower than substrate, as shown in Fig. 4 and summarized in Table 1. This result is in accordance with de Souza et al. (2011), and is tightly connected with the layer's porosity. In such a situation, elastic modulus depends on the pore fraction, following, at a first approximation, the law of mixtures (Meyers and Chawla, 1999). By considering the elastic modulus of "dense" titanium dioxide as ~200 GPa (Hanaor and Sorrell, 2011; Meyers and Chawla, 1999), the variation in the anodic layers was approximately 80%.

For the heat and hydrothermal treatment a very strong effect on elastic modulus is observed, this indicates a change in structure of the layers. In spite of the pores effects, the elastic modulus values for the heat treated surfaces (Fig. 4 and Table 1) is much higher than for AO samples, presenting profiles closer to the Ti substrate value (~145 GPa). The increase in elastic modulus of the treated layers indicates a

higher cohesion inside the layer due change in bonding for these samples. Also is observed a decrease in porous size (Fig. 1) which reveals a change in the morphology and homogeneity induced by heat and hydrothermal treatments.

The increase in crystallinity after heat and hydrothermal treatments, as well as the precipitation of rutile can be responsible for part of change in mechanical properties. As hardness, elastic modulus of rutile is higher than the anatase one (Hanaor and Sorrell, 2011), affecting the average elastic response of the surface. Among the thermal treatments, the surfaces showed no significant differences in the profiles of elastic modulus as a function of contact depth. The AO+HT surfaces presented the highest values of elastic modulus. The large error bars in elastic modulus are somewhat due to the aforementioned inaccuracies in the determination of the "zero" contact depth, though in minor degree. As hardness depends on the inverse of the contact area A_c, elastic modulus is inversely proportional to the square root of A_c (Oliver and Pharr, 2004). The inhomogeneous distribution of rutile precipitates affected the dispersion of results, but in a different way than it was for hardness. Data in Fig. 4 correspond to the averaged elastic modulus, calculated from several indentations, each of them interacting with a small volume under the surface and different precipitates concentrations.

The representative load-unload curves of the thermal treated samples (Fig. 5) shows that layers heat treated behaves differently than hydrothermal treated. The recovery load rate of heat treated layers is higher than hydrothermal which might have been due to the rutile phase that has higher values of elastic modulus than anatase and it is in higher quantity on heat treated layers. Although the results show that heat treated samples had different values of penetration depth compared to hydrothermal treated, this effect might have happened because of the large fluctuations in the hardness and elastic modulus profiles as seen in Fig. 4 that were also displayed in loading-unloading curves.

Considering materials for implants, the elastic modulus should be as close as possible to the values of the human bone. If the elastic modulus is much higher than the bone, a stress concentration occurs in the interface bone-implant which causes bone atrophy named stress shielding (Niinomi and Nakai, 2011; Niinomi, 1998). However, when concerning to the wear of a biomaterial, it is important that the implant presents good adhesion, high hardness and high toughness to decrease abrasion residues generated during the functional loadings that are harmful if released in the human body.

3.3.2. Scratch tests analysis

Tip profile penetration during scratch tests on the studied samples, using nanoindenter equipment, and the SEM micrographs are shown in Fig. 6. AO samples had their layer easily broken and removed from the substrate and the profile shows a large fluctuation in tip penetration values during and after the tests. Additionally, AO+HT layers presented a distinct behavior compared to AO (Fig. 6b) with SEM images of the scratch exhibiting a more ductile layer but also presenting debris of material left on the edges and a lower a fluctuation for penetration values. Consequently the AO+HT layers are less brittle than AO layers and the deformation presents a
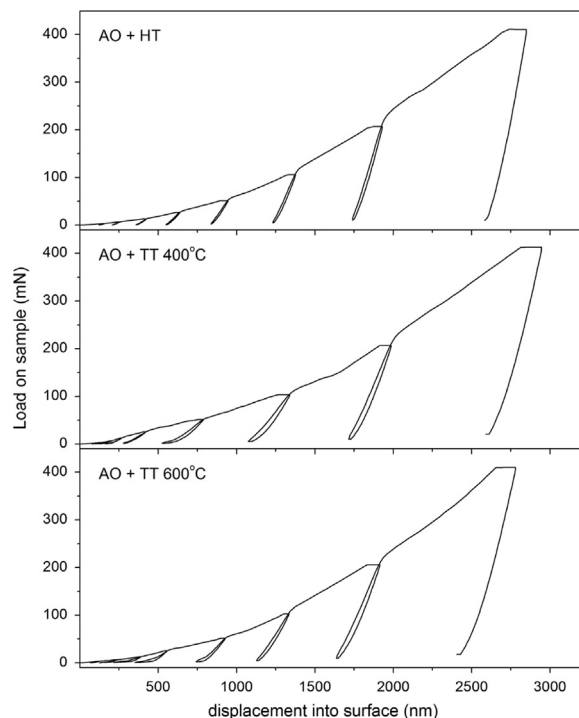

Fig. 5 – Load–unload curves of the nanoindentation tests under multi-cycled mode at the applied load of 400 mN for samples thermal treated.

more ductile profile. The regions were fluctuations on the profiles occur are closely related to the location where the ripping of the material occurs as observed by SEM images.

For the samples with posterior heat treatment AO+TT400 °C and AO+TT600 °C, the release of the material does not occur at the beginning of the scratch and its quantity of debris decreased for the sample treated at the higher temperature. Then the film has a higher cohesion than the AO and AO+HT. The plastic deformation and fracture become more severe from around the scratch distance 400 μm, which corresponds to 220 mN applied load The maximum depth of penetration achieved for the AO+TT600 °C sample was 2 μm and 2.5 μm for the AO+TT400 °C. The tip penetration when the maximum load is applied is lower for the heat treated samples (AO+ TT400 °C – AO+600 °C) compared to AO and AO+HT samples. In addition, the number of cracks and debris inside and at edges of the scratches decreased as the temperature of heat treatment increases. As previously stated, hardening of these studied layers occurs due to thermal treatment which increases the cohesion of the film, the morphology of pores and the amounts of rutile phases (Alves et al., 2013; Kung et al., 2012; Tao et al., 2009).

3.3.3. Tribology

The presented images shown in Fig. 7 correspond to SEM tracks produced by tribology tests in anodic layers with thermal and hydrothermal treatments, and the corresponding friction coefficient profiles. The SEM track shows that AO+HT and AO+TT400 °C surfaces have similar behaviors and friction coefficient profiles. It can be seen an increase in track width and the film was partially removed as evidenced by EDS analysis, occurring a deposit of debris at the edges. In
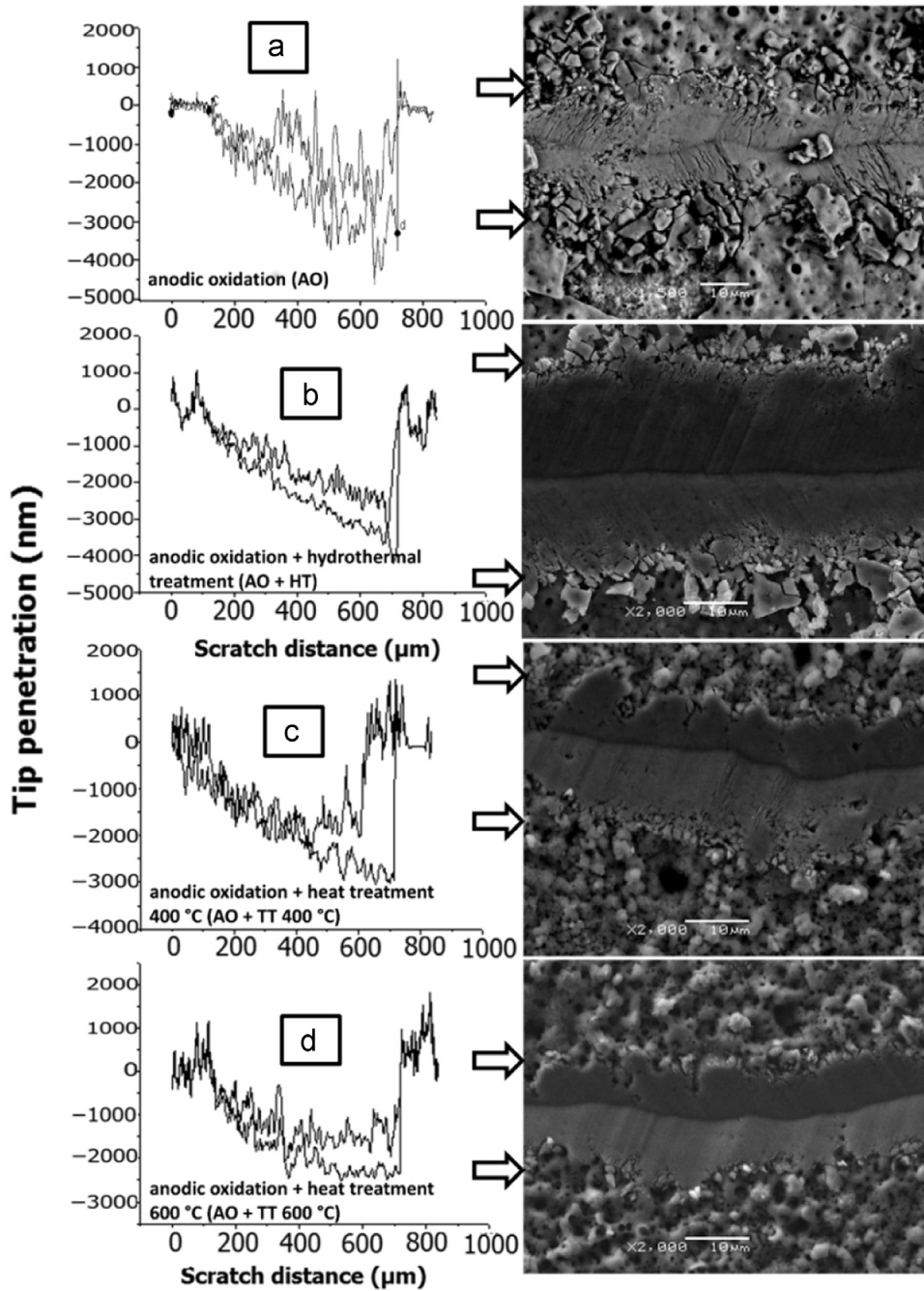
Fig. 6 – Tip penetration profiles of scratch tests performed on the AO (a), AO+HT, (b) AO+TT400 °C (c), AO+TT600 °C (d) samples obtained during scratching and after load removal. The SEM micrographs were obtained at approximately 200 mN on the applied load.

addition, for AO+400 °C sample the width of the wear track was narrow compared to AO+HT. The presence of Ca and P was not detected in the center of the track indicating that for AO+HT samples the layer has been greatly removed exposing the substrate. The low resistance to long-term wear conditions is attributed to hydrothermal treatment according results in literature (Alsaran et al., 2011; Vangolu et al., 2011). The adhesion plays an important role in wear properties; with weak adhesion an easy disruption of oxide layer occurs. The hydrothermal treated oxide layers have probably weak adhesion leading to abrasive loosen particles and these

abrasive effects causes bonding with the counter body. The adhesion of MAO coatings affects the wear resistance and the most important disadvantage is the low resistance in long-term wear conditions (Vangolu et al., 2011).

In the case of AO+TT400 °C layers the decrease on friction coefficient at 2000–4000 laps of the test could be explained by the wear debris that might be transferred to the counter surface, which causes a soft-soft surface contact and the friction coefficient and abrasive effect decreases. At heat treatment temperature of 600 °C which corresponds to AO+TT600 °C surfaces, the behavior of the wear is noticeable.
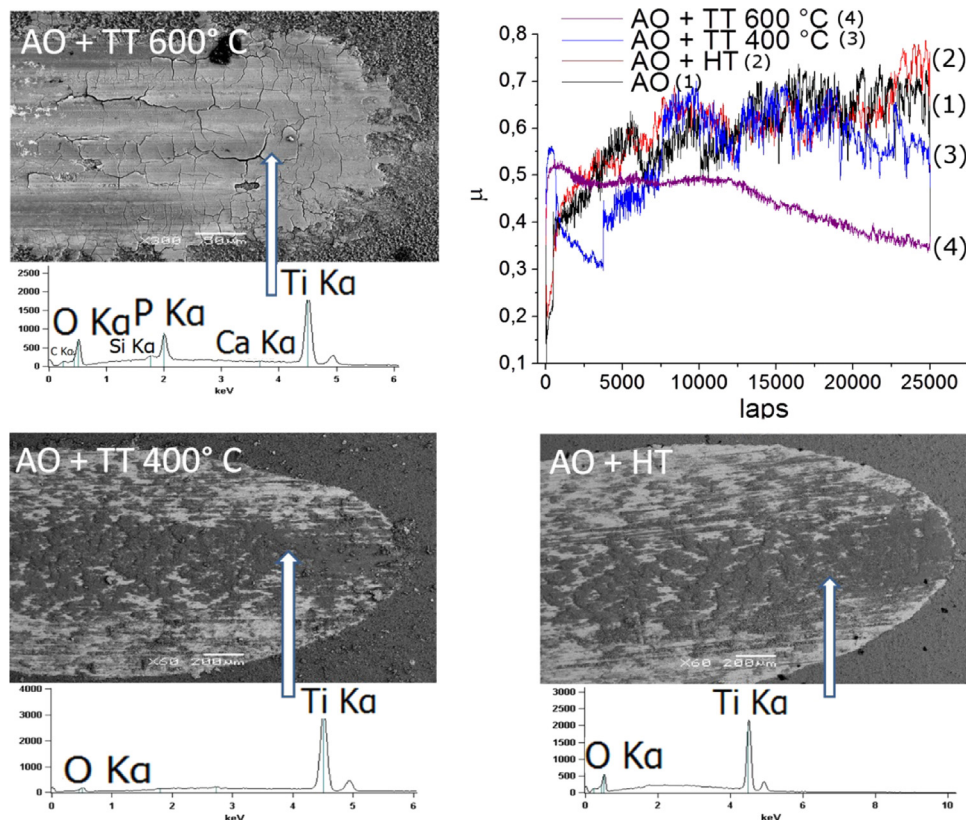
Fig. 7 – SEM track images produced by tribology tests for the studied samples. The EDS of the track regions are indicated. Top-right-corner, profile of the friction coefficient for different treatments.

The layer was not removed during wear test indicating a good response for conditions that need long term life under contact to other bodies. However cracks and a start of detachment of the film along the entire track were observed. By EDS analysis along the trail, the elements of Ca and P still remains which are constituents of the oxidized film studied. In addition, the middle of the track shows light regions where only titanium was found which indicates that no presence of the film was found in these regions, only the substrate. The heat treated layer at 600 °C is relatively stable, decreasing the wear resistance and friction coefficient graphs with further reduction which might be due to the adhesively bond to the counter surface. Based on SEM images it can be concluded that the samples AO+TT600 °C were unique, and the layer was still on the surface after test. However, the AO+TT400 °C samples shows that at the beginning of its profile it is observed similar behavior to AO+600 °C but the film degrades with increasing number of oscillations and from 5000 laps the substrate is probably reached and a similar comportment to the oxidized samples and hydrothermal treatment are observed.

These results confirm that crystallization of the Ti phases due to thermal treatments also affects the tribological characteristics of the layers. Moreover, with increasing the crystallinity the layers are more resistant, which is also evidenced on profile penetration of scratch tests Fig. 6. Even if the AO+600 °C samples presents cracks and detachment, for the number of cycles that it was subjected, these are positive results as the tribological test is a simulated long-term effect

of an implant in the human body. In the case of heat treated samples, there is an increase in friction resistance mainly due to the improved adhesive layer and the rolling resistance of surface asperities with an overall wear mechanism of abrasion.

The values of the wear rates for the studied surfaces presented in Table 1, shows for hydrothermal treatment similar values to standard oxide layers. Heat treatments however, had lower values of wear rate. Among the heat treatments, AO+TT600 °C had the lowest value of wear rate which can be explained along with the SEM image (Fig. 7) since the layer does not remove from the surface.

Table 1 also presents the H/E ratio values, which is related to the elastic strain to failure and is suitable for predicting wear resistance (Dao et al., 2007; Musil, 2012). H/E ratio values can also be compared in terms of number of cracks left by nanoindenter tests and wear rate values (Musil, 2012). H/E values for AO+HT layers obtained the lowest values, which reiterates the instability of this layer, exhibiting an intense cracking left by nanoindenter and the highest value of wear rate for the studied samples. Heat treated layers however, slightly increases the H/E values as the temperature rises. Less cracking and lower values of wear are presented on AO+TT600 °C layers, which presented the most mechanically stable films of this investigation. AO layers on the other hand obtained the highest value of H/E with the largest standard deviation which is possibly due to the rich CaP regions and it is in accordance with its lower wear rate values.
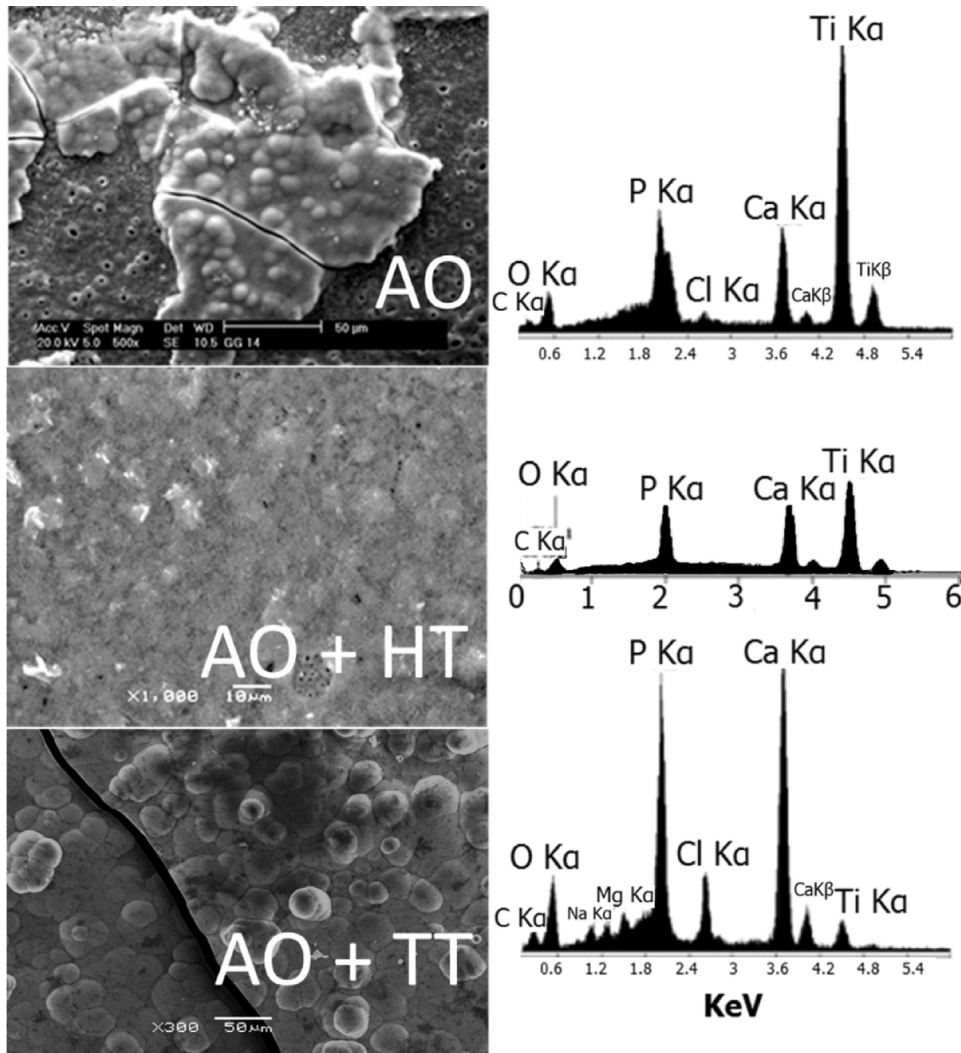
Fig. 8 – SEM micrographs showing the morphology of samples after testing in SBF AO. Followed by the EDS spectra of the studied samples after soaked in SBF;

3.4. SBF tests

In vitro bioactivity tests was performed using simulated body fluid (SBF) soaking the samples for 21 days at 37 °C. Fig. 6 shows the images taken by SEM surface of the studied samples. A new layer with globular morphology is formed on the surface of AO samples (Fig. 8). However, the apatite layer was not entirely covered and exhibit parts of the standard layer in different regions.

The AO+HT samples present a layer without the previous globular morphology but similar results have been reported for hydrothermal treatment (Cimenoglu et al., 2011; Song et al., 2010). The morphology exhibits nano-sized crystallites that are HAp, which might have a different morphology due to the different ratio of Ca and P on the anodic layer. However, it covered all the surface layer compared to standard samples.

Analyses carried out to determine the elements present in this new layer are shown in the EDS spectra (Fig. 7). All surfaces contained calcium and phosphorus; calcium phosphate thus formed on the anodic film. The globular morphology observed in the oxidized surface is indicative of formation of hydroxyapatite. Similar morphologies have been reported in the literature (Cui et al., 2009; Jonasova et al., 2002; Yang et al., 2004).

For the heat treatment samples similar morphology and globular nucleation layer to the AO samples was observed. Using the values of Ca and P given by EDS, the ratio Ca/P was determined and resulting in 1.60 ± 0.09, which is a value close to the expected for hydroxyapatite (1.63), confirming that the layer formed corresponds to hydroxyapatite. The whole sample surface was covered with hydroxyapatite.

Authors have shown that heat treatment might reduce the surface bioactivity (D. Wei et al., 2007), amount of HAp in vitro tests, due to the release of Ca and P components onto the SBF. They observed an increase in crystallinity of Ca and P components when increasing the heat treatment, this effect caused a slower release of the Ca–P components onto the surface in vitro SBF tests, which caused an inability of forming HAp. However, the results presented here shown contrary behaviors which might have been due to the strong layer produced with no variation on the diffusion of these components onto the surface owing to the no appearance of any Ca–P crystalline components on XRD.
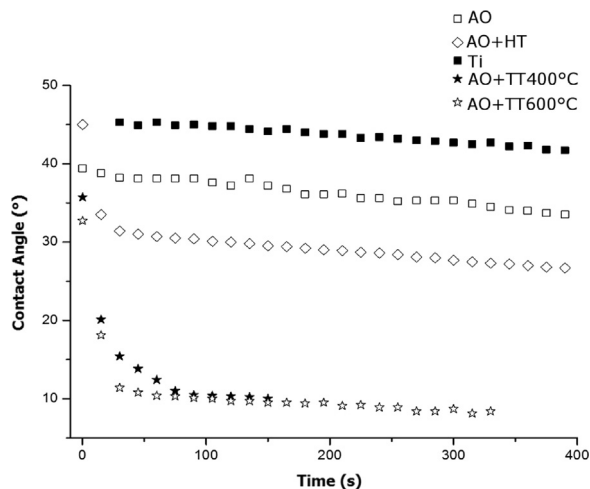
Fig. 9 – Wettability measures for the studied surfaces.

3.5.   Wettability

The results of wettability are shown in Fig. 9. The tests were done by measuring the contact angle of the SBF drop on different surfaces. The images shown in Fig. 10 are the optical images of contact angles when the droplet reaches 300 s in the Fig. 9, which is the stabilization point for all of the analyzed layers. The AO samples had lower values ($\theta_{AO} = 36°$) of contact angle compared to pure titanium ($\theta_{Ti}=43°$) which is due to the porosity of the surface, as observed by SEM images. Several studies in the literature (Castner and Ratner, 2002) relates that a higher porosity influences the wettability of the surfaces, so there is greater cell proliferation and a more intimate contact with the biological liquid, which provides greater interaction with proteins and cells. In addition, for titanium alloys, the solution drop contact angle seems to be inversely related to surface roughness (Kubiak et al., 2011).

The contact angle profile to the surface with hydrothermal treatment remains similar to surfaces without heat treatment in the first minutes and decreases with time ($\theta_{HT}=30°$).
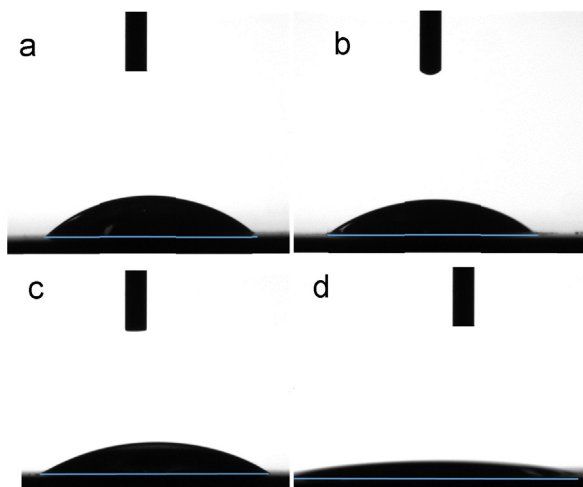

Fig. 10 – Optical images of the contact angles of (a) substrate, (b) AO, (c) AO+HT and (d) AO+TT600 °C.

These values of the contact angles resulted from the morphology and composition of this area.

There is a large difference between the surfaces with hydrothermal and heat treatments. Surfaces with heat treatments suffered a sharp drop compared to the hydrothermal treatment and also with the surfaces without heat treatment. In the first few seconds there is a large decrease in the values, and becomes constant after 10 s. The lower values of contact angle on anodic layers after heat treatment ($\theta_{HT}=11°$) could be related to the high temperature treatment which promotes mobility of oxygen and oxygen vacancy sites in the TiO$_2$ oxide lattice. The transition of oxygen and vacancy sites produces charges in MAO TiO$_2$, this causes dissociative adsorption of the water molecules on the surface (Perron et al., 2007). These vacancy sites are kinetically more favorable for OH groups which promote increased for water adsorption on TiO$_2$ surface (Lu et al., 2000; Ma et al., 2012). Consequently, the hydrophilicity of anodic layers is greatly improved and the contact angle is significantly reduced, indicating that this surface is suitable to interact with the human body. The increase in wettability improves the relationship between the surface of the implant and the biological environment.

4.   Conclusions

- The surface layer here produced exhibited morphologies with similar roughness but varying in porosity size and distribution. After thermal treatment rutile phases was identified. EDS analysis indicated that the Ca and P were presented in the structure with increasing content of Ca for hydrothermal treatment giving a Ca/P ratio of 1.6.
- Mechanical properties of thermal treated present higher values of elastic modulus compared to the standard anodic oxidized layer which were attributed to better cohesion of the layers and can be related to rutile precipitation hardening of these treatments. In addition, a slightly increase in hardness were perceived after the heat treatments with decrease in the number of cracks and improved behavior on scratch tests. Wear values for samples submitted to posterior heat treatment were lower than for the standard anodic layer. Additionally, anodic layers submitted to 600 °C were the only ones who maintained the layer after the test.
- Bioactivity assessed in vitro using SBF proved that these surfaces are bioactive showing nucleation of HAp after 21 days of immersion. Heat treated samples exhibited hydrophilic surfaces which were attributed to the thermal treatment that produces vacancy sites favorable to OH groups and consequently increases the water adsorption on these anodic layers.
- The methodology here proposed for production AO samples rich in Ca–P and submitted to heat treatments can be considered an improvement for biomedical applications since it greatly improves the required properties for bioactive coatings.

Acknowledgments

REFERENCES

Alsaran, A., Purcek, G., Hacisalihoglu, I., Vangolu, Y., Bayrak, Ö., Karaman, I., Celik, A., 2011. Hydroxyapatite production on ultrafine-grained pure titanium by micro-arc oxidation and hydrothermal treatment. Surf. Coat. Technol. 205, S537–S542.

Alves, A.C., Oliveira, F., Wenger, F., Ponthiaux, P., Celis, J.-P., Rocha, L.A., 2013. Tribocorrosion behaviour of anodic treated titanium surfaces intended for dental implants. J. Phys. D. Appl. Phys. 46, 404001.

Arslan, E., Totik, Y., Demirci, E.E., Efeoglu, I., 2013. Wear and adhesion resistance of duplex coatings deposited on Ti6Al4V alloy using MAO and CFUBMS. Surf. Coat. Technol. 214, 1–7, http://dx.doi.org/10.1016/j.surfcoat.2012.10.006.

Castner, D.G., Ratner, B.D., 2002. Biomedical surface science: foundations to frontiers. Surf. Sci. 500, 28–60.

Chen, J., Shi, Y., Wang, L., Yan, F., Zhang, F., 2006. Preparation and properties of hydroxyapatite-containing titania coating by micro-arc oxidation. Mater. Lett. 60, 2538–2543.

Cimenoglu, H., Gunyuz, M., Kose, G.T., Baydogan, M., U⤹gurlu, F., Sener, C., 2011. Micro-arc oxidation of Ti6Al4V and Ti6Al7Nb alloys for biomedical applications. Mater. Charact. 62, 304–311, http://dx.doi.org/10.1016/j.matchar.2011.01.002.

Cui, X., Kim, H.-M., Kawashita, M., Wang, L., Xiong, T., Kokubo, T., Nakamura, T., 2009. Preparation of bioactive titania films on titanium metal via anodic oxidation. Dent. Mater. 25, 80–86.

Cummings, S.R., Melton, L.J., 2002. Epidemiology and outcomes of osteoporotic fractures. Lancet 359, 1761–1767.

Dao, M., Lu, L., Asaro, R.J., De Hosson, J.T.M., Ma, E., 2007. Toward a quantitative understanding of mechanical behavior of nanocrystalline metals. Acta Mater. 55, 4041–4065, http://dx.doi.org/10.1016/j.actamat.2007.01.038.

de Souza, G.B., Mikowski, A., Lepienski, C.M., Foerster, C.E., 2010. Indentation hardness of rough surfaces produced by plasma-based ion implantation processes. Surf. Coat. Technol. 204, 3013–3017, http://dx.doi.org/10.1016/j.surfcoat.2010.03.001.

de Souza, G.B., de Lima, G.G., Kuromoto, N.K., Soares, P., Lepienski, C.M., Foerster, C.E., Mikowski, A., 2011. Tribo-mechanical characterization of rough, porous and bioactive Ti anodic layers. J. Mech. Behav. Biomed. Mater. 4, 796–806.

Fischer-Cripps, A.C., 2011. Nanoindentation. Springer Science & Business Media, New York.

Flaherty, J.H., Liu, M.L., Ding, L., Dong, B., Ding, Q., Li, X., Xiao, S., 2007. China: the aging giant. J. Am. Geriatr. Soc. 55, 1295–1300, http://dx.doi.org/10.1111/j.1532-5415.2007.01273.x.

Hanaor, D.A.H., Sorrell, C.C., 2011. Review of the anatase to rutile phase transformation. J. Mater. Sci. 46, 855–874.

Ishizawa, H., Ogino, M., 1995. Formation and characterization of anodic titanium oxide films containing Ca and P. J. Biomed. Mater. Res. 29, 65–72.

Jin, F., Chu, P.K., Wang, K., Zhao, J., Huang, A., Tong, H., 2008. Thermal stability of titania films prepared on titanium by micro-arc oxidation. Mater. Sci. Eng. A 476, 78–82.

Jin, K., Simpkins, J.W., Ji, X., Leis, M., Stambler, I., 2015. The critical need to promote research of aging and aging-related diseases to improve health and longevity of the elderly population. Aging Dis. 6 (1), 1–5, http://dx.doi.org/10.14336/AD.2014.1210.

Jonasova, L., Müller, F.A., Helebrant, A., Strnad, J., Greil, P., 2002. Hydroxyapatite formation on alkali-treated titanium with different content of Na+ in the surface layer. Biomaterials 23, 3095–3101.

Kasemo, B., 1983. Biocompatibility of titanium implants: surface science aspects. J. Prosthet. Dent. 49, 832–837.

Kokubo, T., Takadama, H., 2006. How useful is SBF in predicting in vivo bone bioactivity?. Biomaterials 27, 2907–2915.

Korkusuz, P., Korkusuz, F., 2004. Hard tissue-biomaterial interactions. Biomater. Orthop., 1–40.

Kubiak, K.J., Wilson, M.C.T., Mathia, T.G., Carval, P., 2011. Wettability versus roughness of engineering surfaces. Wear 271, 523–528.

Kumar, K.N.P., 1995. Growth of rutile crystallites during the initial stage of anatase-to-rutile transformation in pure titania and in titania-alumina nanocomposites. Scr. Metall. Mater. 32, 873–877, http://dx.doi.org/10.1016/0956-716X(95)93217-R.

Kung, K.-C., Yuan, K., Lee, T.-M., Lui, T.-S., 2012. Effect of heat treatment on microstructures and mechanical behavior of porous Sr–Ca–P coatings on titanium. J. Alloy. Compd. 515, 68–73, http://dx.doi.org/10.1016/j.jallcom.2011.11.050.

Laurindo, C.A.H., Torres, R.D., Mali, S.A., Gilbert, J.L., Soares, P., 2014. Incorporation of Ca and P on anodized titanium surface: Effect of high current density. Mater. Sci. Eng. C. Mater. Biol. Appl. 37, 223–231, http://dx.doi.org/10.1016/j.msec.2014.01.006.

Li, H.X., Rudnev, V.S., Zheng, X.H., Yarovaya, T.P., Song, R.G., 2008. Characterization of Al2O3 ceramic coatings on 6063 aluminum alloy prepared in borate electrolytes by micro-arc oxidation. J. Alloy. Compd. 462, 99–102.

Li, L.-H., Kim, H.-W., Lee, S.-H., Kong, Y.-M., Kim, H.-E., 2005. Biocompatibility of titanium implants modified by microarc oxidation and hydroxyapatite coating. J. Biomed. Mater. Res. Part A 73, 48–54.

Liu, S., Yang, X., Cui, Z., Zhu, S., Wei, Q., 2011. One-step synthesis of petal-like apatite/titania composite coating on a titanium by micro-arc oxidation. Mater. Lett. 65, 1041–1044.

Liu, X., Chu, P.K., Ding, C., 2004. Surface modification of titanium, titanium alloys, and related materials for biomedical applications. Mater. Sci. Eng. R Rep. 47, 49–121.

Lu, G., Bernasek, S.L., Schwartz, J., 2000. Oxidation of a poly-crystalline titanium surface by oxygen and water. Surf. Sci. 458, 80–90, http://dx.doi.org/10.1016/S0039-6028(00)00420-9.

Ma, C., Nagai, A., Yamazaki, Y., Toyama, T., Tsutsumi, Y., Hanawa, T., Wang, W., Yamashita, K., 2012. Electrically polarized micro-arc oxidized TiO2 coatings with enhanced surface hydrophilicity. Acta Biomater. 8, 860–865, http://dx.doi.org/10.1016/j.actbio.2011.09.021.

Meyers, M.A., Chawla, K.K., 1999. Mechanical Behavior of MaterialsPrentice Hall. New Jersey, vol. 72.

Montazeri, M., Dehghanian, C., Shokouhfar, M., Baradaran, A., 2011. Investigation of the voltage and time effects on the formation of hydroxyapatite-containing titania prepared by plasma electrolytic oxidation on Ti–6Al–4V alloy and its corrosion behavior. Appl. Surf. Sci. 257, 7268–7275.

Musil, J., 2012. Hard nanocomposite coatings: thermal stability, oxidation resistance and toughness. Surf. Coat. Technol. 207, 50–65, http://dx.doi.org/10.1016/j.surfcoat.2012.05.073.

Niinomi, M., 1998. Mechanical properties of biomedical titanium alloys. Mater. Sci. Eng. A 243, 231–236.

Niinomi, M., 2008. Mechanical biocompatibilities of titanium alloys for biomedical applications. J. Mech. Behav. Biomed. Mater. 1, 30–42.

Niinomi, M., Nakai, M., 2011. Titanium-based biomaterials for preventing stress shielding between implant devices and bone. Int. J. Biomater., 2011, http://dx.doi.org/10.1155/2011/836587.

Oliver, W.C., Pharr, G.M., 2004. Measurement of hardness and elastic modulus by instrumented indentation: Advances in understanding and refinements to methodology. J. Mater. Res. 19, 3–20.

Park, I.S., Woo, T.G., Jeon, W.Y., Park, H.H., Lee, M.H., Bae, T.S., Seol, K.W., 2007. Surface characteristics of titanium anodized

in the four different types of electrolyte. Electrochim. Acta 53, 863–870.

Peine, A., Faulkner, A., Jæger, B., Moors, E.H.M., 2015. Science, technology and the "grand challenge" of ageing—Understanding the socio-material constitution of later life. Technol. Forecast. Soc. Change.http://dxdoi.org/10.1016/j.techfore.2014.11.010.

Perron, H., Vandenborre, J., Domain, C., Drot, R., Roques, J., Simoni, E., Ehrhardt, J.-J., Catalette, H., 2007. Combined investigation of water sorption on TiO_2 rutile (110) single crystal face: XPS vs. periodic DFT. Surf. Sci. 601, 518–527.

Ryu, H.S., Song, W.-H., Hong, S.-H., 2008. Biomimetic apatite induction of P-containing titania formed by micro-arc oxidation before and after hydrothermal treatment. Surf. Coat. Technol. 202, 1853–1858.

Saha, R., Nix, W.D., 2002. Effects of the substrate on the determination of thin film mechanical properties by nanoindentation. Acta Mater. 50, 23–38.

Serrano, M., Blasco, M.A., 2007. Cancer and ageing: convergent and divergent mechanisms. Nat. Rev. Mol. Cell Biol. 8, 715–722.

Shen, D., Cai, J., Guo, C., Liu, P., 2013. Evolution of residual stresses in micro-arc oxidation ceramic coatings on 6061 Al alloy. Chin. J. Mech. Eng. 26, 1149–1153, http://dx.doi.org/10.3901/CJME.2013.06.1149.

Song, H.J., Kim, J.W., Kook, M.S., Moon, W.J., Park, Y.J., 2010. Fabrication of hydroxyapatite and TiO_2 nanorods on microarc-oxidized titanium surface using hydrothermal treatment. Appl. Surf. Sci. 256, 7056–7061, http://dx.doi.org/10.1016/j.apsusc.2010.05.024.

Spurr, R.A., Myers, H., 1957. Quantitative Analysis of Anatase-Rutile Mixtures with an X-Ray Diffractometer. Anal. Chem. 29, 760–762, http://dx.doi.org/10.1021/ac60125a006.

Tao, X.J., Li, S.J., Zheng, C.Y., Fu, J., Guo, Z., Hao, Y.L., Yang, R., Guo, Z.X., 2009. Synthesis of a porous oxide layer on a multifunctional biomedical titanium by micro-arc oxidation. Mater. Sci. Eng. C 29, 1923–1934.

Vangolu, Y., Alsaran, A., Yildirim, O.S., 2011. Wear properties of micro arc oxidized and hydrothermally treated Ti6Al4V alloy in simulated body fluid. Wear 271, 2322–2327, http://dx.doi.org/10.1016/j.wear.2010.12.039.

Wei, D., Zhou, Y., Jia, D., Wang, Y., 2007a. Effect of heat treatment on the structure and in vitro bioactivity of microarc-oxidized (MAO) titania coatings containing Ca and P ions. Surf. Coat. Technol. 201, 8723–8729.

Wei, J., Yoshinari, M., Takemoto, S., Hattori, M., Kawada, E., Liu, B., Oda, Y., 2007b. Adhesion of mouse fibroblasts on hexamethyldisiloxane surfaces with wide range of wettability. J. Biomed. Mater. Res. Part B Appl. Biomater. 81, 66–75.

Yang, B., Uchida, M., Kim, H.-M., Zhang, X., Kokubo, T., 2004. Preparation of bioactive titanium metal via anodic oxidation treatment. Biomaterials 25, 1003–1010.

Yang, T.-C., Shu, H.-Y., Chen, H.-T., Chung, C.-J., He, J.-L., 2014. Interface between grown osteoblast and micro-arc oxidized bioactive layers. Surf. Coat. Technol. 259, 185–192.

Zhou, R., Wei, D., Yang, H., Feng, W., Cheng, S., Li, B., Wang, Y., Jia, D., Zhou, Y., 2014. MC3T3-E1 cell response of amorphous phase/TiO_2 nanocrystal composite coating prepared by microarc oxidation on titanium. Mater. Sci. Eng. C 39, 186–195.